An ODE whose solutions contain all knots and links

ROBERT W. GHRIST
Center for Applied Mathematics, Cornell University, Ithaca, NY 14853

PHILIP J. HOLMES
Program in Applied & Computational Mathematics and
Department of Mechanical & Aerospace Engineering
Princeton University, Princeton, NJ 08544-1000

Dedicated to L. P. Shil'nikov on the occasion of his sixtieth birthday.

To appear in *Intl. J. Bifurcation and Chaos.*

Abstract

Periodic orbits of a third order ODE are topological knots. Using results from the theory of branched 2-manifolds, we prove the existence of simple ODEs whose periodic orbit set contains every type of knot and collection of knots (link). The construction depends on the dynamics near certain configurations of Shil'nikov connections, and can be applied to, among other things, a model of a nonlinear electric circuit.

1 Introduction and Main Results

A *knot* is a simple closed curve in a three dimensional space. A collection of periodic orbits of a three dimensional flow forms a disjoint union of knots, or a *link*, the topology of which can illuminate the global structure of solutions of the underlying differential equation. For example, in [HW85, Hol86, Hol89], knot invariants are used to study bifurcation sequences in which "chaotic" flows having positive topological entropy are created, by varying a parameter, from simple flows supporting merely one or two periodic orbits. As another example, certain types of knots can force positive topological entropy in a nonsingular flow [Mor78, Wad89]. Here, however, we are concerned rather with ODEs as machines for building interesting families of infinite links.

It is not difficult to produce a simple ODE whose periodic orbit set is infinite: the well-known Lorenz equations,

$$\begin{aligned} \dot{x} &= \sigma(y-x) \\ \dot{y} &= \rho x - y - xz \\ \dot{z} &= -\beta z + xy, \end{aligned} \tag{1}$$

will do. At certain parameter values, periodic solutions to these equations form a link of infinitely many components (though these are unstable and very difficult to find!). See [GW79] for an analysis of the similar "geometric" Lorenz system or [MM95] for new results on Eqn. (1). Many other systems which exhibit "chaotic" behavior have attractors filled with infinite collec-

tions of unstable periodic orbits.

Two knots are said to be *equivalent* or of the same *knot type* if one can smoothly deform one knot to the other without cutting, as if one were deforming a knotted loop of rope — a more precise definition would be that the two knots are *isotopic* [Rol77]:

Definition 1 *Two subsets, A and B, of $\mathbb{R}^n$ are* isotopic *if there exists a homeomorphism $\phi : \mathbb{R}^n \to \mathbb{R}^n$ such that $\phi(A) = B$.*

Given an ODE, one generally wants to know how many and which types of knots and links are present. In [FW85], very general hypotheses (e.g., positive topological entropy plus some smoothness) are given under which a three dimensional flow must contain periodic orbits exhibiting infinitely many distinct knot types. It follows that the solutions to (1), for certain parameter values, support an infinite number of distinct knot types. However, it must be noted that not all types are necessarily present. For example, the analysis of [BW83a] shows that only a restricted class of knot types appear in the geometric Lorenz attractor.

Given the differential equation $\dot{x} = f(x)$ for $x \in \mathbb{R}^3$, we wish to answer the following basic question:

Question 1 *Can the periodic orbits of f contain every type of knot?*

In §2, we will review the basic tools of *branched 2-manifolds* (or *templates*) and relate Question 1 in this new setting to Conjecture 1, stated in §2, which first appeared in [BW83b]. In §3 and §4, we present some symbolic tools and outline the resolution of Conjecture 1, the details of which will appear in [Ghr95]. In §5, we apply our results on branched 2-manifolds to ODEs which support a particular type of global connections, first studied by Shil'nikov [Shi65, Shi70]. This will allow us to derive our main results:

Theorem 1 *There exists an open set U in the space of C^1 vector fields on $\mathbb{R}^3$ such that the periodic orbit set of each vector field $f \in U$ contains representatives from every knot and link isotopy class.*

We also provide a specific example:

Theorem 2 *There exists an open set of parameters $\beta \in [6.5, 10.5]$ for which periodic solutions to the differential equation*

$$\begin{aligned} \dot{x} &= 7[y - \phi(x)], \\ \dot{y} &= x - y + z, \\ \dot{z} &= -\beta y, \\ \phi(x) &= \frac{2}{7}x - \frac{3}{14}\left[|x+1| - |x-1|\right], \end{aligned} \tag{2}$$

contain representatives from every knot and link equivalence class.

Theorem 1 can be interpreted as a knot-theoretic analogue to the existence of ODEs with complicated dynamics which are nevertheless structurally stable. Theorem 2 is a simple example of an equation, originally due to Chua et al. [CKM86], which supports a certain type of homoclinic connection. This sort of connection, first studied by Shil'nikov [Shi65, Shi70], provides the important link between the topological results on branched 2-manifolds of §4 and physically relevant differential equations. A more detailed analysis of the template structure near Shil'nikov connections is given in the Appendix.

Throughout this paper, we restrict attention to the class of *tame* knots and links; that is, those simple closed curves which are isotopic to simple closed polygons in $\mathbb{R}^3$ [Rol77, BZ85]. This excludes infinitely iterated structures such as *solenoids* or *wild knots*. On the other hand, using a finitely iterated structure will be seen in §4 to be vital to our results.

2 Templates for Flows

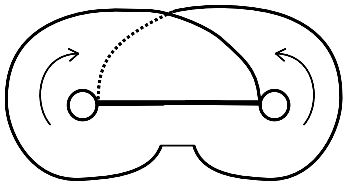

FIGURE 1: The Lorenz template

When investigating a third-order ODE numerically, one often finds an apparent *attractor*, onto which the dynamics rapidly collapses. For example, Lorenz [Lor63] noted the structure of the attractor for Eqn. (1): it appears to be a two-sheeted surface on which there is a unidirectional flow about each "strip" (cf. Fig. 1). This notion of a multi-sheeted surface was made precise by Williams in the late seventies [Wil74, Wil79] and later named a *template*.

Definition 2 *A* template *(also known as a* knotholder*) is a compact branched two-manifold fitted with a smooth expansive semiflow and built from a finite number of* joining *and* splitting charts*, as in Fig. 2.*

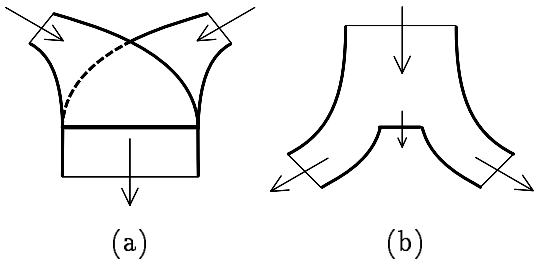

FIGURE 2: (a) joining and (b) splitting charts

The Lorenz template, $\mathcal{L}$, displayed in Fig. 1, is the simplest nontrivial example of a template. The dynamics on a template is a "semiflow" since it only goes one way and is not reversible like a true flow. Note also that the semiflow is "overflowing" through the gap in the branch line; however, since no periodic orbits (i.e., knots) can ever leave the template, we are not concerned with this condition (cf. orbits which exit a Smale horseshoe after a finite number of iterates). As such, we will "cut back" the overflowing segment of a splitting chart along the semiflow until reaching the branch line (see Fig. 3). This will produce an equivalent template composed of "strips" connecting the branch lines. The expansivity condition refers to the fact that nearby orbits must eventually separate. Of course, one may construct templates which are a good deal more complicated than $\mathcal{L}$ — we will in fact do so shortly.

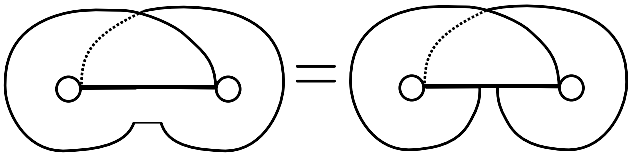

FIGURE 3: Equivalent templates

The connection between templates and ODEs is expressed in the Template Theorem of Birman and Williams:

Theorem 3 (Birman and Williams, 1983) *Given a flow on a three-manifold having a hyperbolic chain-recurrent set (i.e., Axiom A plus no-cycle), the periodic orbits are in one-to-one correspondence with the periodic orbits on a particular template (with at most two exceptions). On any finite sublink, this correspondence is via isotopy.*

The interested reader may consult [Bow78, Sma67, GH83] for definitions and [BW83b, GHS95] for the proof of this important result. The hypothesis is essentially one of hyperbolicity: there must exist uniformly contracting and expanding directions along the entirety of the dynamically relevant subset of the flow. The template is formed by identifying all orbits which share the same asymptotic future. That is, one

collapses out along the stable direction along the original flow, transforming the flow on a three-dimensional manifold to a semiflow on a branched two-dimensional manifold. Occasionally, one must modify the flow before collapsing, giving rise to at most two fictitious orbits [BW83b]. None of the templates appearing in this work will require any such modification.

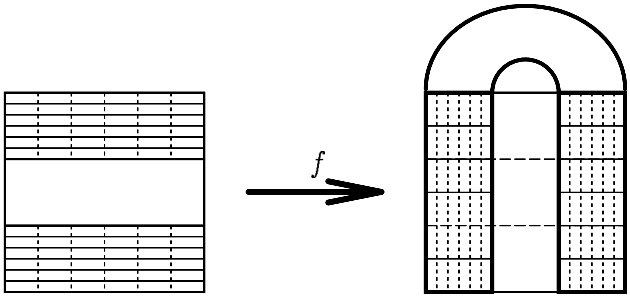

FIGURE 4: The Smale horseshoe map

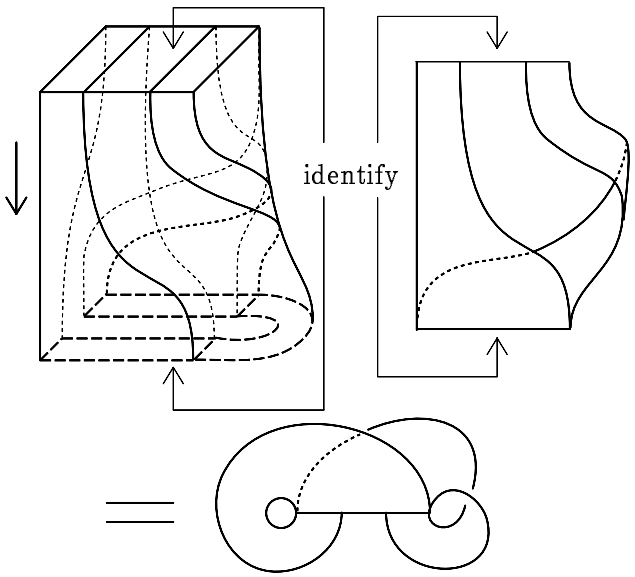

FIGURE 5: The suspended horseshoe reduced to a template

We give an example of this procedure, which appeared first in the analysis of Holmes and Williams [HW85] (see also [Hol86, Hol89, GH93, GHS95]): the suspended Smale horseshoe. Let $f : D^2 \to D^2$ be the standard horseshoe map acting on a 2-disc (see Fig. 4). The *suspension* of this map involves identifying a point $x \in D^2$ with its image $f(x)$ in distinct copy of D^2 and placing a translation flow "in between" the two discs. This suspension now gives a flow on a solid torus $D^2 \times S^1$ which has f as a Poincaré map. Horseshoes arise naturally in Poincaré maps of certain relevant systems such as periodically forced oscillators, whose phase spaces are $D^2 \times S^1$. The horseshoe is a hyperbolic map with stable and unstable directions which are, respectively, horizontal and vertical (note Fig. 4). Hence, we may collapse out the stable directions to obtain a template $\mathcal{H}$: the *horseshoe template.*

Fig. 5 illustrates the reduction to $\mathcal{H}$. The reader will note that $\mathcal{H}$ is similar to the Lorenz template $\mathcal{L}$ except for a half-twist along the rightmost strip. The addition of the single twist radically affects the types of knots which are present [HW85].

Given a template $\mathcal{T}$, one wants to find what types of knots live on $\mathcal{T}$. This is by no means a simple task, but it is a great deal easier than working in the unreduced three-dimensional flow. In their original work on templates, Birman and Williams posed the following conjecture, which is the template version of Question 1:

Conjecture 1 (Birman and Williams, 1983) *There does not exist an embedded template which supports all knot types as periodic orbits of the semiflow: i.e., a* universal template.

After partial results were obtained by M. Sullivan [Sul94], this conjecture was resolved in the negative by Ghrist [Ghr95]. In §4 we will present a rough idea of the proof in order to explain the techniques, which are applicable to other templates which are derived from ODEs. In §5

we will show that the universal template constructed in §4 appears near symmetric spiral connections of Shil'nikov type, thereby proving Theorems 1 and 2.

3 Symbolic Structures for Templates and Renormalizations

Our primary tools for working with templates are symbolic dynamics [Bow78, GH83] and kneading theory for one-dimensional maps [MT77, Wil79, Wil77]. Given a template $\mathcal{T}$, there are a finite number of one-dimensional branch lines $\{\ell_j : j = 1..M\}$ and a finite number of two-dimensional strips $\{x_i : i = 1..N \geq 2M\}$ connecting these in the appropriate manner. Under this labeling scheme, each orbit which remains on $\mathcal{T}$ has associated to it a unique semi-infinite sequence in the x_i-symbols specified by the order in which the orbit traverses the various strips. Alternatively, one can associate the x_i-symbols to the subsets of the branch lines from which the strips emanate: then, these *branch segments* $\{x_1, \ldots, x_N\}$ form a Markov partition for the one-dimensional return maps induced by the semiflow on the branch lines. These symbol sequences are denoted *itineraries*, and the collection of all itineraries for $\mathcal{T}$ is the *itinerary space*,

$$\begin{aligned} \Sigma_{\mathcal{T}} &= \{\mathbf{a} = a_0 a_1 a_2 \ldots : \quad (3) \\ &\qquad \mathbf{a} \text{ is an itinerary of an orbit on } \mathcal{T}\} \\ &\subset \{x_1, x_2, \ldots, x_N\}^{\mathbf{Z}^+} . \end{aligned}$$

The dynamics on the template are captured symbolically by the action of the *shift operator*:

$$\sigma(a_0 a_1 a_2 a_3 \ldots) = a_1 a_2 a_3 \ldots . \qquad (4)$$

Not every possible string of symbol sequences may appear in a given template, since there may be restrictions on where one can travel. These are expressed in an N by N *transition matrix*, $A_{\mathcal{T}}$, where

$$A_{\mathcal{T}}(i,j) = \begin{cases} 0: & \nexists \text{ a strip from } x_i \text{ to } x_j \\ 1: & \exists \text{ a strip from } x_i \text{ to } x_j \end{cases} . \qquad (5)$$

An itinerary is said to be *admissible* with respect to $A_{\mathcal{T}}$ if the symbol sequence $a_0 \ldots a_i a_{i+1} \ldots$ satisfies

$$A(a_i, a_{i+1}) = 1 \quad \forall i. \qquad (6)$$

Lemma 1 *Given a template $\mathcal{T}$ with Markov partition $\{x_i : i = 1..N\}$ and transition matrix $A_{\mathcal{T}}$, the set of all admissible sequences under $A_{\mathcal{T}}$ is precisely $\Sigma_{\mathcal{T}}$.*

Proof: this correspondence is identical to the description of hyperbolic sets via Markov partitions and subshifts of finite type [Bow78, GH83]. □

A fair amount of information about a template can be stored in symbolic form. For example, we can easily specify all the boundary components of a template. One other tool which helps to describe a template has connections with the kneading theory of Milnor and Thurston [MT77, Wil79, Wil77]. In essence, we wish to place a coordinate system on each branch line ℓ_j and then order itineraries in such a way as to accurately reflect their "physical" ordering of points on each ℓ_j.

This procedure is simplest for orientable templates: let $\mathcal{T}$ be an orientable template with Markov partition $\{x_1, \ldots, x_N\}$ and branch lines $\{\ell_1, \ldots, \ell_M\}$. Choose an orientation on each ℓ_j so that all the branch segments x_i on ℓ_j have an induced ordering, denoted $\lhd$. Then, given two itineraries in $\Sigma_{\mathcal{T}}$ which commence from the same branch line, one orders them lexicographically with respect to $\lhd$. For nonorientable templates, like $\mathcal{H}$, the matter requires a bit more bookkeeping, but is nonetheless well-defined [HW85, Hol89, GH93]. All of the templates appearing in this section and in §4 will be orientable.

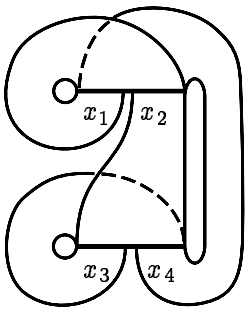

FIGURE 6: The template $\mathcal{V}$

An example will best serve to illustrate the symbolic descriptions. Let $\mathcal{V}$ denote the template of Fig. 6, outfitted with the Markov partition $\{x_i : i = 1..4\}$ as shown. The ordering $\lhd$ is chosen on the branch lines to be

$$\mathcal{V} \quad \begin{array}{ll} \ell_1 : & x_1 \lhd x_2 \\ \ell_2 : & x_3 \lhd x_4 \end{array} . \tag{7}$$

Now a lexicographic ordering on $\Sigma_{\mathcal{V}}$ gives the appropriate ordering of orbits. *Example:* $x_1^2 x_2 x_3 x_4 \ldots \lhd x_1 x_2 x_3 x_4 \lhd x_1 x_2 x_4 \ldots$. In addition, we can specify the boundary of $\mathcal{V}$, $\partial(\mathcal{V})$, as the left (∂^ℓ) and right (∂^r) endpoints under $\lhd$ of all itineraries commencing with each x_i: that is, the left and right edges of each x_i strip,

$$\partial(\mathcal{V}) = \left\{\partial_i^\ell, \partial_i^r : i = 1..4\right\} \tag{8}$$

$$\begin{array}{ll} \partial_1^\ell(\mathcal{V}) = (x_1)^\infty & \partial_1^r(\mathcal{V}) = x_1 (x_2 x_4)^\infty \\ \partial_2^\ell(\mathcal{V}) = x_2 (x_3)^\infty & \partial_2^r(\mathcal{V}) = (x_2 x_4)^\infty \\ \partial_3^\ell(\mathcal{V}) = (x_3)^\infty & \partial_3^r(\mathcal{V}) = x_3 (x_4 x_2)^\infty \\ \partial_4^\ell(\mathcal{V}) = x_4 (x_1)^\infty & \partial_4^r(\mathcal{V}) = (x_4 x_2)^\infty \end{array}$$

Given a symbolic description of a template $\mathcal{T}$ and its orbits, we wish to address the question of which types of knots $\mathcal{T}$ supports. Of necessity, this will require the examination of periodic orbits whose periods are arbitrarily large: a daunting task given only pencil, paper, and finite visual skills. We use two constructions to assist in this task. The first is the notion of a *subtemplate*, first introduced in the study of the horseshoe template $\mathcal{H}$ by Holmes [Hol89]:

Definition 3 *A* subtemplate $\mathcal{S} \subset \mathcal{T}$ *of a template* $\mathcal{T}$ *is a topological subset of* $\mathcal{T}$ *which, with the restriction of the semiflow of* $\mathcal{T}$*, satisfies the definition of a template (Definition 2).*

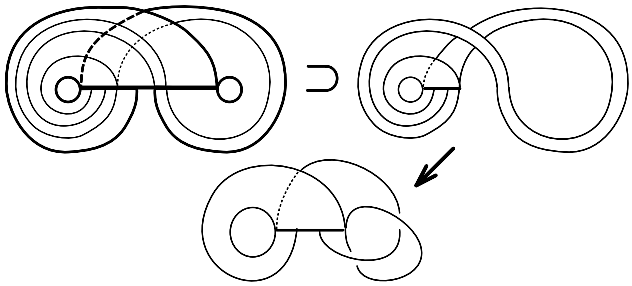

FIGURE 7: A subtemplate of $\mathcal{L}$

A subtemplate of the Lorenz template $\mathcal{L}$ is pictured in Fig. 7. When the subtemplate is cut along the boundary and removed from $\mathcal{L}$, it is itself a template. Of course, one can construct subtemplates which are very complicated. The particular subtemplate of Fig. 7 is special in that it is diffeomorphic to the original $\mathcal{L}$ (though embedded differently). This suggests the second key notion, that of a *template renormalization*:

Definition 4 *A* template renormalization *of a template* $\mathcal{T}$ *is a map* $\mathfrak{R} : \mathcal{T} \hookrightarrow \mathcal{T}$ *taking orbits to orbits which is a diffeomorphism onto its image.*

.

The terminology for Definition 4 derives from the renormalization theory for one-dimensional maps [Fei78, PTT87, GH83]. The branch lines of $\mathcal{T}$ form a Poincaré section for the semiflow which induce a set of coupled one-dimensional return maps. The image of a template renormalization gives a renormalization of the return maps in the sense that we have chosen distinguished subintervals of the branch lines [PTT87].

The image of a template renormalization is by definition a subtemplate. The existence of a template renormalization allows one to iterate

the procedure, obtaining an increasingly complicated sequence of embedded subtemplates, each of which is diffeomorphic to the original. When combined with the itinerary space $\Sigma_{\mathcal{T}}$, we can reduce the construction of these subtemplates to a simple action on the Markov partition:

Lemma 2 *A template renormalization $\mathfrak{R} : \mathcal{T} \hookrightarrow \mathcal{T}$ induces a map $\mathfrak{R} : \Sigma_{\mathcal{T}} \hookrightarrow \Sigma_{\mathcal{T}}$ whose action is to inflate each element of the Markov partition $\{x_i : i = 1..N\}$ to a finite admissible word $\{\mathbf{w}_i = w_1 w_2 \dots w_{n(i)} : i = 1..N\}$ in the x_i-symbols.*

Proof: by Definition 4, $\mathfrak{R}$ maps the branch lines of $\mathcal{T}$ into the branch lines of $\mathcal{T}$. Hence, each strip of $\mathcal{T}$ (corresponding to a symbol x_i of the Markov partition) is mapped to a finite sequence of strips in $\mathcal{T}$, corresponding to a finite admissible word $\mathbf{w}_i$. □

As an example, consider again the renormalization $\mathfrak{L} : \mathcal{L} \hookrightarrow \mathcal{L}$ of Fig. 7. This map has the following action on the Markov partition:

$$\mathfrak{L} : \mathcal{L} \hookrightarrow \mathcal{L} \qquad \begin{cases} x_1 \mapsto x_1 \\ x_2 \mapsto x_1 x_2 \end{cases} . \qquad (9)$$

The action of this map on any individual orbit is easily calculated: e.g., $\mathfrak{L}\left(x_1 x_2^2\right)^\infty = \left(x_1^2 x_2^2\right)^\infty$. Note that a template renormalization $\mathfrak{R}$ also has a topological action since it takes knots to knots. However, in so doing, it will typically change the knot type. When this does not happen, we have the following:

Definition 5 *An* isotopic renormalization *of an embedded template $\mathcal{T}$ is a template renormalization $\mathfrak{R}$ such that $\mathfrak{R}(\mathcal{T})$ is isotopic to $\mathcal{T}$: that is, $\mathfrak{R} : \mathcal{T} \hookrightarrow \mathcal{T}$ extends to a diffeomorphism of $\mathbb{R}^3$.*

An isotopic template renormalization preserves the knot types of the individual orbits. We will exploit isotopic template renormalizations to specify arbitrarily complicated subtemplates while retaining information about the knot types of the individual orbits. Given the additional symbolic data, all of these subtemplates have nice coordinates within the space $\Sigma_{\mathcal{T}}$.

4 Universal Templates

The first example of an isotopic template renormalization was discovered by M. Sullivan:

Lemma 3 (M. Sullivan [Sul94]) *The following renormalization of $\mathcal{V}$ is isotopic:*

$$\mathfrak{D} : \mathcal{V} \hookrightarrow \mathcal{V} \qquad \begin{cases} x_1 \mapsto x_1 \\ x_2 \mapsto x_1 x_2 \\ x_3 \mapsto x_3 \\ x_4 \mapsto x_3 x_4 \end{cases} . \qquad (10)$$

Proof: see Fig. 8. □

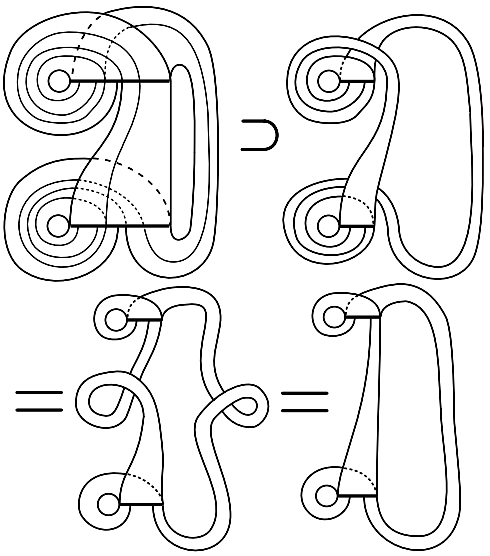

FIGURE 8: The action of $\mathfrak{D}$

Hence, there exists an infinite sequence of subtemplates of $\mathcal{V}$, each of which is isotopic to the original. As shown in [Ghr95], there actually exists an infinite sequence of *disjoint, unlinked* copies of $\mathcal{V}$ inside itself. As can be seen, this behavior depends upon the existence of *mixed*

crossings within the template $\mathcal{V}$, where we give a crossing a positive or negative sign according to Fig. 9.

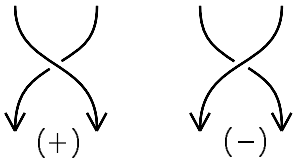

FIGURE 9: The sign of a crossing

Even more surprising is the following result of [Ghr95], the proof of which we outline here:

Theorem 4 *The template $\mathcal{V}$ contains an isotopic copy of every knot and link as periodic orbits of the semiflow.*

Outline of proof:

Step 1: braids and the theorem of Alexander

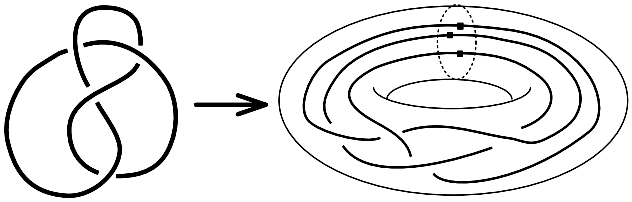

FIGURE 10: The figure-eight knot and its braid form

We organize all knots and links into a manageable form via the use of *closed braids*. A *closed braid on P strands*, b, is a collection of a finite number of disjoint simple closed curves placed inside of a standardly embedded solid torus $D^2 \times S^1$ such that every cross section $D^2 \times \{\theta\}$ intersects b transversally in precisely P points. It is a theorem of Alexander [Ale23] that each knot or link is isotopic to some closed braid on P strands for some P: Fig. 10 gives an example, the *figure-eight knot*. There is an strong analogy between the use of knot and link theory in the study of ODEs and the use of braid theory in the study of surface maps [Boy94, Boy84], the latter having the advantage of an additional algebraic structure.

Step 2: the templates $\mathcal{W}_q$

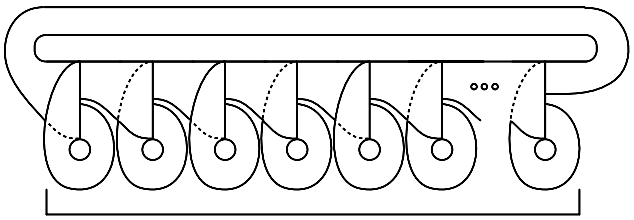

FIGURE 11: The template W_q

Fig. 11 displays a member of a family of templates denoted $\{\mathcal{W}_q\}$ for q a positive integer. Note that $\mathcal{W}_1$ is identically $\mathcal{V}$ and that increasing q by one has the effect of adding two *ears* to one side. Note that the ears alternate in sign: that is, the way in which they cross over or under the rest of $\mathcal{W}_q$ (cf. Fig. 9). In [Ghr95], the algebraic structure of closed braids is used to establish the following:

Lemma 4 *Given any closed braid b, an isotopic copy of b exists as a (set of) periodic orbit(s) on some $\mathcal{W}_q$ for q sufficiently large.*

The proof depends crucially upon the fact that the ears of $\mathcal{W}_q$ alternate in their sign (as per Fig. 9): whether they cross over or under the remainder of the template. Then, one creates crossings of either sign between arbitrary pairs of strands yielding generators of the braid group.

Step 3: appending an ear

In order to build $\mathcal{W}_{q+1}$ from $\mathcal{W}_q$, one must "append" a pair of ears in the appropriate place. Our strategy is to start with a renormalized copy of $\mathcal{W}_1 \subset \mathcal{V}$ (similar to the situation of Fig. 8) and append a pair of ears to obtain $\mathcal{W}_2$, which

is again renormalized, etc. Appending an ear can be accomplished by the following procedure, illustrated for a positive ear in Fig. 12:

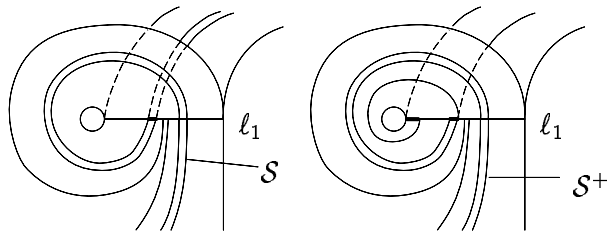

FIGURE 12: Appending an ear

Lemma 5 *Given a subtemplate $\mathcal{S} \subset \mathcal{V}$ which does not contain the orbit $(x_1)^\infty$ (resp. $(x_3)^\infty$), one can append an ear to the $\lhd$-minimal interval of $\mathcal{S} \cap \ell_1$ (resp. ℓ_2), yielding a new subtemplate $\mathcal{S}^+$.*

Recall that ℓ_1 and ℓ_2 refer to the upper and lower (resp.) branch lines of $\mathcal{V}$.

Step 4: finding $\mathcal{W}_q$ within $\mathcal{V}$ for all $q > 0$

This is by far the most difficult step, for in order to produce $\mathcal{W}_{q+1}$, we must find a copy of $\mathcal{W}_q \subset \mathcal{V}$ which avoids the orbits $(x_1)^\infty$ and $(x_3)^\infty$. This is done by employing "deep" renormalizations of $\mathcal{V}$ and carefully tracking the positions of $\mathcal{W}_q \subset \mathcal{V}$ via the $\lhd$-coordinates in order to apply Lemma 5.

Proposition 1 *The inflation*

$$\mathfrak{H} : \mathcal{V} \hookrightarrow \mathcal{V} \quad \begin{cases} x_1 \mapsto x_2 x_3^2 x_4 x_1 (x_2 x_4)^2 x_2 x_3 x_4 x_1 \\ x_2 \mapsto x_2 x_3^2 x_4 x_1 (x_2 x_4)^3 x_2 x_3 x_4 x_1 \\ x_3 \mapsto x_2 x_3^2 x_4 x_1 x_2 x_4 \\ x_4 \mapsto x_2 x_3^2 x_4 x_1 x_2 x_4 \end{cases}, \tag{11}$$

takes $\mathcal{V}$ to $\mathfrak{H}(\mathcal{V})$ isotopically such that $\mathcal{S} \equiv \mathfrak{H}(\mathcal{V}) \subset \mathcal{V}$ satisfies Lemma 5, permitting one to append an ear near $(x_1)^\infty$ along $\mathfrak{H}(\partial_2^\ell(\mathcal{V})) \cap \ell_1$.

The renormalization $\mathfrak{H}$ is derived in [Ghr95] from a composition of simple renormalizations of $\mathcal{V}$, each of whose topological action is via isotopy. To show that the image of the boundary component $\partial_2^\ell(\mathcal{V})$ under $\mathfrak{H}$ satisfies the conditions of Lemma 5, one performs a series of calculations using the $\lhd$-ordering. A proposition very like Proposition 1 also applies, allowing the addition of an ear near $(x_3)^\infty$ after a similar renormalization $\mathfrak{H}^*$.

To complete the proof that $\mathcal{W}_q \subset \mathcal{V}$ for all $q > 0$, we begin with $\mathcal{W}_1 = \mathcal{V}$ as a (trivial) subtemplate of $\mathcal{V}$, and iterate the following procedure $q - 1$ times:

1. Send $\mathcal{V}$ along with the subtemplate $\mathcal{W}_i$ into $\mathcal{V}$ isotopically via $\mathfrak{H}$.
2. Append an ear to the subtemplate $\mathcal{W}_i$ near $(x_1)^\infty$, obtaining a new subtemplate W_i^+.
3. Send $\mathcal{V}$, and along with it the subtemplate $\mathcal{W}_i^+$, into $\mathcal{V}$ isotopically via $\mathfrak{H}^*$.
4. Append an ear to the subtemplate $\mathcal{W}_i^+$ near $(x_3)^\infty$, obtaining a new subtemplate $\mathcal{W}_{i+1}$.

One must carefully calculate that at each stage, one adds the proper type of ear at the appropriate position. Because of the complexity of $\mathfrak{H}$, the subtemplates $\mathcal{W}_q$ are impossible to visualize — to appreciate this, the reader is encouraged to attempt a picture of $\mathfrak{H}(\mathcal{V}) \subset \mathcal{V}$. The details of this construction are contained in [Ghr95], and a complete exposition of the symbolic methods will be given in [GHS95].

Given any knot or link, we can by Step 1 isotope it to a closed braid. According to Step 2, this closed braid appears on the template $\mathcal{W}_q$ for some q. Finally, since, by Step 4, $\mathcal{W}_q$ is a subtemplate of $\mathcal{V}$ for any q, we conclude that the knot or link lives on $\mathcal{V}$. In fact, coupled with the remark following Lemma 3, we have proved that $\mathcal{V}$ contains *infinitely many isotopic copies* of every knot and link. □

Theorem 4 resolves Conjecture 1 in the negative and is an interesting result from the point of view

of pure topology. However, our present concern is to use this result to comment on the topological structures which exist within simple vector fields on $\mathbb{R}^3$.

5 Spiral Connections

To construct a template for a flow is a relatively difficult undertaking: given a generic ODE exhibiting complicated behavior, there is no way of knowing a priori whether a template for the attractor exists, much less what its structure might be. Templates have of late have appeared in a number of papers on time-series analysis, in which an attractor is approximated by a template in a rather *ad hoc* fashion [MSN+91, Tuf94, KDTC94]. While this is useful in predicting what sorts of knots may appear within a flow, there is no guarantee that such knots actually exist. Hence, if we wish to conclude the existence of a universal template within a flow, we must be careful to satisfy the requirements of Theorem 3.

We recall a construction, originally due to L. P. Shil'nikov, which will allow us to conclude the existence of templates embedded within the attractor for certain simple flows on $\mathbb{R}^3$. The following theorem was first proven by Shil'nikov [Shi65, Shi70], with extensions and repetitions later in [Tre84] and elsewhere. A number of textbooks also contain these results along with proofs [GH83, Wig88, Wig90].

Theorem 5 (L. P. Shil'nikov) *Let $\dot{x} = f(x)$ for $x \in \mathbb{R}^3$ be a third order ODE which satisfies the following two conditions:*

1. *There exists a fixed point p for the vector field, and the linearization $Df|_p$ at p has eigenvalues $\{-\lambda^s \pm \omega i, \lambda^u\}$, with*

$$\lambda^u > \lambda^s > 0 \qquad \omega \neq 0. \tag{12}$$

2. *There exists a solution of the flow Γ_t which is* homoclinic *at p. That is, $\lim_{t\to\pm\infty} \Gamma_t = p$. In addition, Γ must be bounded away from all other fixed points.*

Then, there exists a countable infinity of suspended Smale horseshoes in the flow in an arbitrarily small tubular neighborhood of the homoclinic orbit Γ. Under a small C^1 perturbation, finitely many of these horseshoes remain.

The proof of Theorem 5 involves constructing Poincaré sections transversal to Γ near the fixed point p and linearizing the flow near p and along Γ, to obtain approximate return maps. The horseshoes are constructed by flowing pairs of boxes near p and then along Γ. This procedure is outlined in further detail in the Appendix.

The entire flow near Γ does not satisfy the hyperbolicity requirements of Theorem 3: moreover, there are numerous features of the dynamics and (especially) bifurcations of flows near such orbits that are currently unknown. However, the individual horseshoes implied by Theorem 5 *are* hyperbolic, and if we restrict our attention to any such subset of the flow, we may justifiably employ Theorem 3 to obtain a template which captures a *portion* of the flow: that is, orbits on the embedded horseshoe templates are in one-to-one isotopic correspondence with a proper subset of orbits in the flow near Γ.

In the Appendix, we present a "catalogue" of templates which arise from these suspended horseshoes near a Shil'nikov homoclinic orbit. While it is not possible to completely classify the knot and link types of all the orbits which live within the nearby horseshoes, certain facts from the study of the standard horseshoe template $\mathcal{H}$ (as it appears in §2) carry over [HW85, GH93, GHS95].

We now consider a slightly different scenario in which the differential equation $\dot{x} = f(x)$ also has

a symmetry of one of the following forms:

$$\Psi : \begin{array}{l}(x,y,z)\mapsto(-x,-y,-z)\\(x,y,z)\mapsto(-x,-y,z)\end{array} . \qquad (13)$$

Such symmetries are not at all uncommon: the Lorenz system exhibits the second symmetry above [Lor63, GH83]. Now consider a system which has a fixed point, p, satisfying the eigenvalue condition of Eqn. (12) and which has an orbit , which tends to p in negative time and to $\Psi(p)$ in positive time. The system will then take on the appearance of Fig. 13, displaying either a pair of homoclinic spirals at $p = \Psi(p)$, or a spiral *heteroclinic cycle* between p and $\Psi(p) \neq p$.

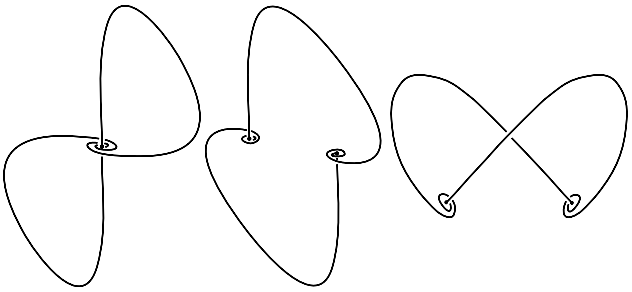

FIGURE 13: Three symmetric homoclinic configurations

Such situations appear in a variety of systems of physical relevance: in models of electric circuits [CKM86, KRC93], in a model of flow through articulated pipes [Cha93], in a model of simple resonance among three coupled oscillators [Wic93], in the Lorenz equations for certain "nonstandard" parameter values [GS86], and in numerous other systems. The standard techniques of using cross sections to construct approximate Poincaré maps has been applied to the configurations of Fig. 13 [GS86, Hol80, BC92], with predictable results, which we restate in a form that suits our purpose:

Theorem 6 *Let $\dot{x} = f(x)$ for $x \in \mathbb{R}^3$ be a third order ODE which satisfies the following three conditions:*

C1 *There exists a fixed point p for the vector field, and the linearization $Df|_p$ at p has eigenvalues $\{-\lambda^s \pm \omega i, \lambda^u\}$, with*

$$\lambda^u > \lambda^s > 0 \qquad \omega \neq 0. \qquad (14)$$

C2 *f respects one of the symmetries of Eqn. (13).*

C3 *There exists a solution of the flow , $_t$ for which $\lim_{t\to-\infty}$, $_t = p$, and $\lim_{t\to+\infty}$, $_t = \Psi(p)$*

Then, there exists a countable infinity of coupled suspended Smale horseshoes (illustrated in Fig. 14) in the flow in arbitrarily small tubular neighborhoods of the connections , and $\Psi($, $)$. Under a small C^1 perturbation, finitely many of these coupled horseshoes remain.

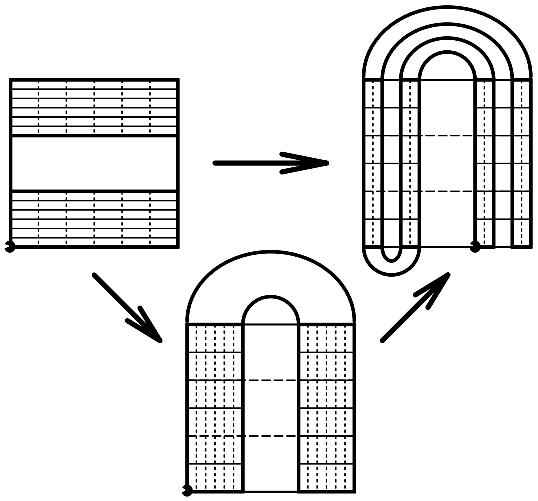

FIGURE 14: The coupled horseshoe map

In order to derive the templates corresponding to these coupled horseshoes, one must be mindful of the exact suspension of the horseshoes. This implies that *local* information about the flow near p and *global* information about the flow along , must be taken into account. For example, the

twist of the homoclinic orbit , outside a neighborhood of p affects the template which is derived in the case of a single homoclinic connection. However, because of the symmetry Ψ, any aberrations due to twisting effects *cancel*: twisting a ribbon once to the left then once to the right undoes any twisting. In the Appendix, we give a detailed construction of this procedure, in order to conclude the following:

Proposition 2 *Given $\dot{x} = f(x)$ satisfying the three requirements of Theorem 6 along with a fourth:*

C4 *Either the homoclinic orbits , and $\Psi(,)$ form a pair of unknotted, unlinked loops joined at p, or the heteroclinic cycle formed by , and $\Psi(,)$ is an unknotted loop (as in Fig. 13).*

Then, there exist a countable infinity of disjoint templates embedded in a tubular neighborhood of , $\cup\, \Psi(,)$, orbits of which are in one-to-one isotopic correspondence with a proper subset of solutions to $\dot{x} = f(x)$. Each of these templates is isotopic to the template $\mathcal{Z}$ in Fig. 15, and finitely many of these templates remain valid under a small C^1 perturbation.

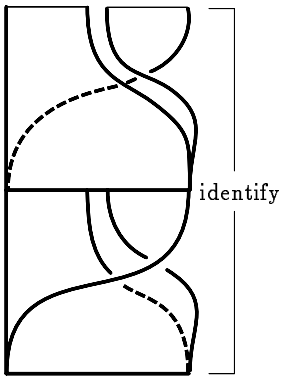

FIGURE 15: The template $\mathcal{Z}$

By examining the subtemplate structure of this template, we will prove the following important result:

Proposition 3 *The template $\mathcal{Z}$ is universal: it contains an isotopic copy of every knot and link.*

Proof: thanks to Theorem 4, we simply need to demonstrate that a subtemplate isotopic to $\mathcal{V}$ is contained within $\mathcal{Z}$. An inflation on symbol sequences $\mathfrak{I} : \Sigma_{\mathcal{V}} \hookrightarrow \Sigma_{\mathcal{Z}}$ generated by

$$\mathfrak{I} : \mathcal{V} \hookrightarrow \mathcal{Z} \qquad \begin{cases} x_1 \mapsto x_2 x_4 \\ x_2 \mapsto x_1 \\ x_3 \mapsto x_4 x_2 \\ x_4 \mapsto x_3 \end{cases} , \qquad (15)$$

defines a subtemplate which is isotopic to $\mathcal{V}$, as illustrated in Fig. 16. *Note:* the symbols x_i in the domain and range of $\mathfrak{I}$ in Eqn. (15) have different meanings as they refer to Markov partitions of different templates. The astute reader will note that the images of the periodic orbits $(x_1)^\infty$ and $(x_3)^\infty \in \mathcal{V}$ map to $(x_2x_4)^\infty = (x_4x_2)^\infty$ in $\mathcal{Z}$: the same orbit. While this precludes the image of the inflation (15) from being diffeomorphic to the domain (as per Definition 4), we may nevertheless disregard this anomaly by "splitting" $\mathcal{Z}$ along $(x_2x_4)^\infty$ and proceeding as usual. The orbit $(x_2x_4)^\infty$ is an unknot and there are plenty of other unknots in the template. □

Corollary 1 *Given a third order system $\dot{x} = f(x)$ which has a pair of symmetric Shil'nikov connections (as per the four conditions* **C1-C4***), every knot and link type lives in an arbitrarily small tubular neighborhood of the Shil'nikov connections. This property persists under small C^1 perturbations.*

Proof: this follows from Propositions 2 and 3, and the structural stability results of Theorem 6. □

The second half of Corollary 1 implies the first of our main results:

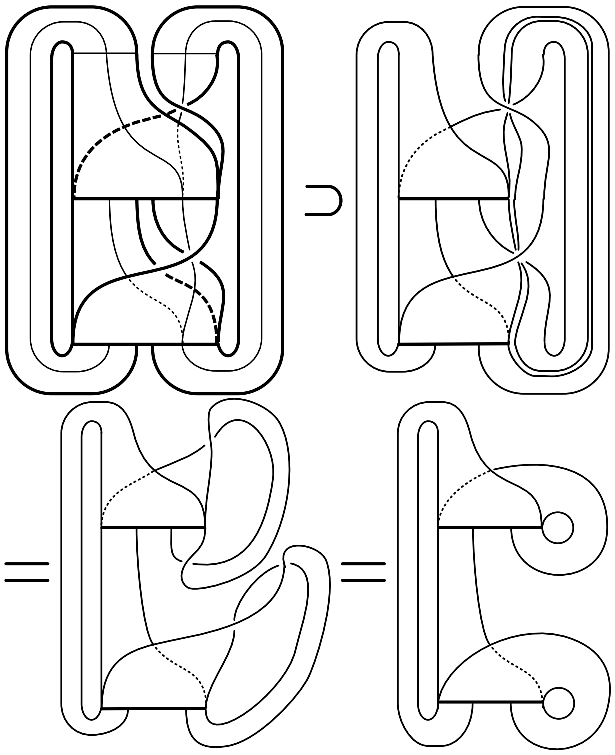

FIGURE 16: $\mathcal{V}$ is a subtemplate of $\mathcal{Z}$

Corollary 2 (Theorem 1) *There exist open sets in the space of C^1 vector fields on $\mathbb{R}^3$ whose periodic orbit set consists of representatives from every link isotopy class.*

The second of our main results follows from the work of Chua et al. [CKM86]:

Corollary 3 (Theorem 2) *There exists an open set of parameters $\beta \in [6.5, 10.5]$ for which periodic solutions to the differential equation*

$$\begin{aligned} \dot{x} &= 7[y - \phi(x)], \\ \dot{y} &= x - y + z, \\ \dot{z} &= -\beta y, \\ \phi(x) &= \frac{2}{7}x - \frac{3}{14}\left[|x+1| - |x-1|\right], \end{aligned} \tag{16}$$

contain representatives from every knot and link equivalence class.

Proof: in [CKM86], it is shown that Eqn. (16) satisfies the four requirements of Theorem 6 and Proposition 2. Corollary 1 gives the result. □

6 Conclusions

The results described in this paper are at once fascinating and depressing. They are mathematically exciting because they provide a tangible link between surprising phenomena in "pure" topology and applied dynamical systems theory, with their implication that simple ODEs modeling physical processes can rather naturally generate all knots and links. They suggest that (collections of) structures of arbitrary global topological complexity can be produced by simple local rules. If such structures in phase space can be mapped into motions in physical space for the devices modeled by these ODEs, then these findings have deep implications for issues of design, control and motion planning.

On the other hand, our results also suggest that the vision developed in [HW85, Hol86, Hol89], cf. [GH93]: that knot and link invariants are useful for the study of orbit genealogies and bifurcation sequences in parameterized dynamical systems, will be limited at best. If an infinite number of copies of *all* knot and link types can occur simultaneously in a flow as ostensibly simple as the double spiral, then they would seem unlikely to serve well as computable indicators to determine different bifurcation routes. We know from the analytical and numerical work of [GS84, GKN84] that the bifurcation structure near Shil'nikov connections is horribly complicated: our results can be interpreted as a topological version of this complexity.

However, here one should note an important distinction between the flows and templates discussed in the present paper and the "simple" horseshoe and Lorenz templates of [BW83a] and [HW85, Hol86, Hol89]. In the latter, all crossings are of the same sign: positive, in the con-

vention of Fig. 9. In contrast, the templates of Figs. 6, 11, and 15, used in the present constructions, contain both positive and negative crossings. Crossings of one sign alone impose severe restrictions on knot and link types, and, roughly speaking, confer a certain "rigidity" on the flow. An important ingredient in the universality proof of §4 is the use of alternating positive and negative crossings in the ears appended to $\mathcal{W}_q$, which permits one to produce arbitrary braid words. This relative freedom appears essential: it also plays a key rôle in M. Sullivan's construction of composite knots with arbitrarily many components [Sul94].

These observations suggest that braid, knot and link structures and their invariants may provide an alternative view of the topological complexity of chaotic dynamical systems, to complement such invariants as topological entropy. (In the opposite direction, Los [Los94] has already suggested the use of dynamical entropy as a knot invariant.) In particular, our present results reveal the surprising structural richness that can result from a particular embedding in phase space of what has now become a canonical object in dynamical systems: Smale's horseshoe. They also provide an interesting coda to the story of homoclinic bifurcations which L. P. Shil'nikov began to tell some thirty years ago.

ACKNOWLEDGEMENTS

This work was completed with the support of a National Science Foundation graduate research fellowship and with Grant DOE DE-FG02-95ER.25238.A000 from the Department of Energy.

A A Catalogue of Templates for Spiral Connections

In this appendix, we will give a detailed account of the templates used in the proof of Proposition 2. The template $\mathcal{Z}$ which is derived is but one of an entire family of templates which appears near spiral Shil'nikov connections. As certain examples of these templates have begun to be observed experimentally from time series data [KDTC94], we feel it is useful to provide a catalogue of which structures occur.

We will begin with the simplest examples in §A.1: namely, those appearing near a single Shil'nikov homoclinic connection. Later, in §A.2, we will examine more intricate families of templates which exist near symmetric Shil'nikov connections. This analysis will establish the existence of the template $\mathcal{Z}$, providing the completion of the proof of Proposition 2.

The "hard" calculations for such systems have been published time and time again (see [Shi65, Shi70] for the originals, [Tre84] for extensions and repetitions and [GH83, Wig88, Wig90] for textbook expositions). As such, we do not reiterate this portion of the analysis, but rather rely on geometric constructions to establish the global geometry of the dynamics near Shil'nikov connections. In the next section, we will give a brief outline of the associated analysis, for the interested reader, based on the standard analysis.

A.1 Single spiral connections

As in Theorem 5, we consider a flow with a fixed point p whose linear spectrum has eigenvalues $\{-\lambda^s \pm \omega i, \lambda^u\}$, with $\lambda^u > \lambda^s > 0$ and $\omega \neq 0$. We also assume the existence of an orbit , , homoclinic to p. The point p has a one-dimensional unstable manifold $W^u(p)$ and a two-dimensional stable manifold $W^s(p)$, along which , $= W^s(p) \cap W^u(p)$ spirals into p. *Remark:* we consider the case where $W^u(p)$ is one-dimensional, but our results apply equally well for $W^u(p)$ two-dimensional and $W^s(p)$ one-dimensional, since this amounts to a reversal of time which leaves periodic orbits invariant.

We are interested in understanding the dynamics near , , and, as is standard, we choose Poincaré

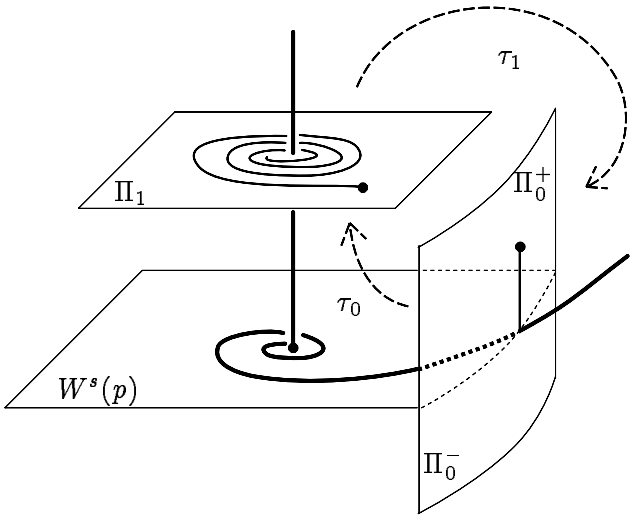

FIGURE 17: Sections near the fixed point p

sections Π_0 and Π_1 transverse to , and sufficiently close to p that the linear analysis below provides a close estimate of the return map. The surface Π_0 is bisected by $W^s(p)$ into upper (Π_0^+) and lower (Π_0^-) halves. Construct a cylindrical coordinate system having origin at p and with Π_0 at constant r and Π_1 at constant $z = \epsilon \ll 1$ (this is the convention of [GH83] — one may just as well choose Π_0 at constant θ [GS84, Wig90]): see Fig. 17. There are two partial return maps: $\tau_0 : \Pi_0^+ \to \Pi_1$, which is concentrated near p, and $\tau_1 : \Pi_1 \to \Pi_0$, which follows along , . By taking Π_0 and Π_1 close enough to p, one can derive a valid approximation for the flow near p by assuming linear behavior:

$$\begin{aligned} r(t) &= r_0 e^{-\lambda^s t} \\ \theta(t) &= \theta_0 + \omega t \\ z(t) &= z_0 e^{\lambda^u t}. \end{aligned} \tag{17}$$

By solving $z(T) = \epsilon$ for T, we obtain the return time for hitting Π_1,

$$T(z) = \frac{1}{\lambda^u} \log \frac{\epsilon}{z}. \tag{18}$$

This gives an analytical expression for the return map τ_0:

$$\tau_0 \;:\; (r_0, \theta, z) \mapsto \left(r_0 \left(\frac{\epsilon}{z}\right)^{\lambda^s/\lambda^u}, \theta + \frac{\omega}{\lambda^u} \log\left(\frac{\epsilon}{z}\right), \epsilon \right). \tag{19}$$

By looking at a sufficiently small neighborhood of , $\cap\, \Pi_1$, one can assume that the return map τ_1 is affine. Hence, there is an analytical expression for the full Poincaré map given by composition of (19) with an affine map which accurately describes the dynamics very close to , . These equations have been analyzed repeatedly [Shi65, Shi70, GS84, GKN84]: we consider a more geometric treatment based on these analyses (cf. [ACT81]).

The action of τ_0 on a segment of constant θ is to stretch it and wrap it around , $\cap\, \Pi_1$ in a logarithmic spiral. Since $z = 0$ is on $W^s(p)$, the image of $\tau_0(r, z)$ as $z \to 0$ approaches , $\cap\, \Pi_1$. This image is then mapped affinely back to Π_0, with $\tau_1(,\ \cap\, \Pi_1) = ,\ \cap\, \Pi_0$: see Fig. 17.

The idea behind the proof of Theorem 5 is to examine the action of $\tau_1\tau_0$ on rectangular strips,

$$B_i = \{(\theta, z) \subset \Pi_0^+ \;:\; a_i \le z \le b_i\}, \tag{20}$$

where the sequences $\{a_i\}$ and $\{b_i\}$ satisfy $a_i < b_i < a_{i-1}$ and $\lim_{i\to\infty} a_i = 0$. For an appropriate choice of numbers $\{a_i, b_i\}$, it can be shown [GH83, Wig88, Wig90] that the image of each pair $\{B_i \cup B_{i+1}\}$ under $\tau_1\tau_0$ intersects $B_i \cup B_{i+1}$ in such a way as to form a hyperbolic horseshoe (see e.g. Theorem 4.8.4 of [Wig90]): see Fig. 18. These pairs form the horseshoes of Theorem 5.

Since these horseshoes are hyperbolic, we can keep track of their stable and unstable foliations. By collapsing one set of these foliations and carefully following the embedding, we will construct the embedded template. We proceed in two steps, according to the two components of the return map $\tau_1\tau_0$.

First, the action of the global map τ_1 is affine and takes the image under τ_0 of the "horizontal" $B_i \subset \Pi_0^+$ to a "vertical" strip in Π_0. Upon

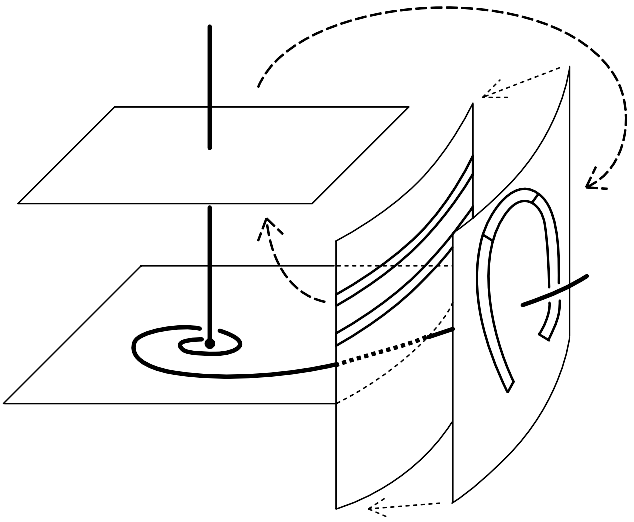

FIGURE 18: The action of τ_1 is affine

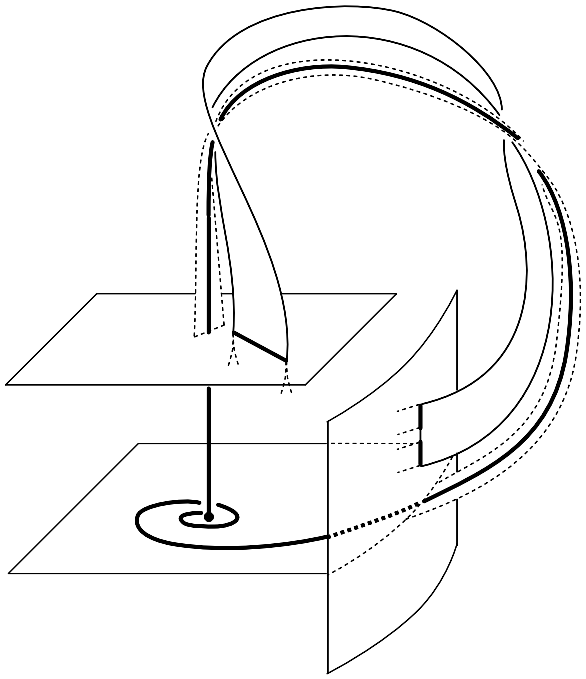

FIGURE 19: Along , , the template is a single strip

collapsing the contracting direction of the map $\tau_0\tau_1$, each box $B_i \subset \Pi_0^+$ becomes a vertical interval $\{a_i \leq z \leq b_i\}$ at a fixed r. Thus, the collapsed B_i and B_{i+1} boxes are disjoint within Π_0^+. Their images, however, are vertical lines which cover Π_0; hence, the two strips are joined together at a branch line.

Since τ_1 is affine, there is no additional folding. Therefore, instead of collapsing the stable direction out to obtain a branch line in Π_0^+, we can propagate the branch line back via τ_1^{-1} to depict the joining of these strips within Π_1, as in Fig. 19. The impact of τ_1 on the topology of the suspension is encoded in the *twist* of , between Π_1 and Π_0^+ (see [CDF90, GW93] for definitions). For N a small tubular neighborhood of , outside a small neighborhood of p, $W^s(p) \cap N$ is a two-dimensional strip which, in between the fixed planes Π_1 and Π_0^+ may "twist" any number of times about , . Since $\tau_1\tau_0(B_i)$ transversally intersects $W^s(p)$, the template will have this same amount of twisting: see again Fig. 19. Given a generic system with a Shil'nikov connection, we cannot say exactly how close to p Π_0 and Π_1 must be chosen for the linear analysis to apply. Hence, we cannot calculate the precise twisting due to the action of τ_1 outside the local neighborhood pf p.

Secondly, the action of the local map, τ_0, is to stretch B_i out along what was the z-direction in Π_0^+ and compress B_i along what was the θ-direction. The image of $\tau_0(\Pi_1^+)$ is a thin spiral (imagine thickening Fig. 17). The image of any consecutive pair B_i, B_{i+1} appears as within a folded strip, reminiscent of a horseshoe: see Fig. 20. As the box $B_i \subset \Pi_1^+$ flows through a neighborhood of p to reach Π_1, it is wrapped around , by an integer number of half-turns, such that B_{i+1} is wrapped around , with one more half-turn than B_i: again, Fig. 20 is crucial in this observation.

More specifically, the particular nature of the winding which occurs near p is revealed by Eqn. (17). As detailed in [Wig88, Wig90], the boxes

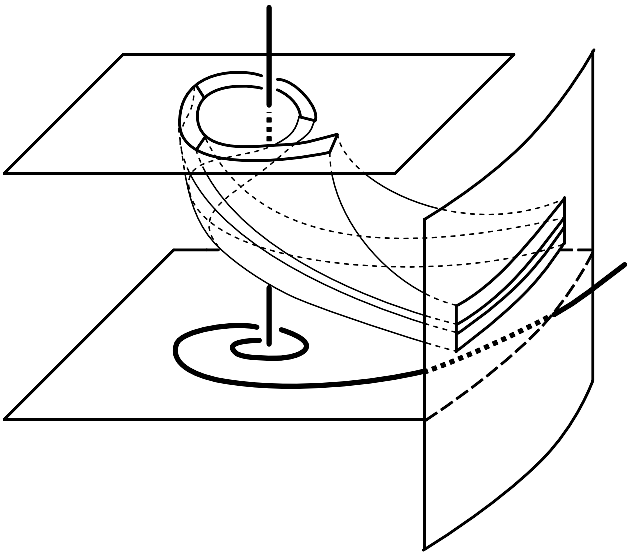

FIGURE 20: A simple horseshoe

B_i can be chosen such that

$$a_i = \epsilon e^{-\pi i \lambda^u/\omega}. \tag{21}$$

Hence,

$$\begin{aligned} \Delta T &\equiv T(a_{i+1}) - T(a_i) \qquad (22)\\ &= \frac{1}{\lambda^u}\left(\log\frac{\epsilon}{a_{i+1}} - \log\frac{\epsilon}{a_i}\right) = \pi, \end{aligned}$$

and the action of the flow of B_{i+1} from Π_0^+ to Π_1 is to wind about , in the θ direction by an additional π, as compared to the motion of B_i. This imparts an additional half-twist to the ensuing template, as per Fig. 20.

Remark: the strips drawn in Fig. 20 have a small amount of twisting; however, there is no guarantee that the "topmost" B_i, which have the least amount of twisting associated with them, satisfy the hyperbolicity conditions. We only know that for i (hence, twist) sufficiently large, pairs of boxes $B_i \cup B_{i+1}$ form hyperbolic horseshoes.

We may now classify the types of horseshoe templates which may appear near , . For i some fixed integer, consider the template formed by collapsing the contracting directions of the flow of the boxes B_i and B_{i+1}. In a neighborhood of p, the strip corresponding to B_i (B_{i+1}) will wind about , with i ($i+1$) half-twists. Then, the strips will join together in Π_1: finally, the strip of the template will follow along , from Π_1 back to Π_0, undergoing M half-twists, for some fixed M.

The template so obtained is a function of the depth of the horseshoe, i, and the fixed global twisting, M. Up to homeomorphism, there are two template types, depending upon the parity of $\alpha \equiv i + M$. The template $\mathcal{H}_\alpha$ is given as in Fig. 21(a): for α even, this is homeomorphic (though not isotopic!) to the standard horseshoe template $\mathcal{H} = \mathcal{H}_0$ (cf. Fig. 5). For any α, $\mathcal{H}_\alpha$ is isotopic to $\mathcal{H}$ with an additional α half-twists inserted after the branch line.

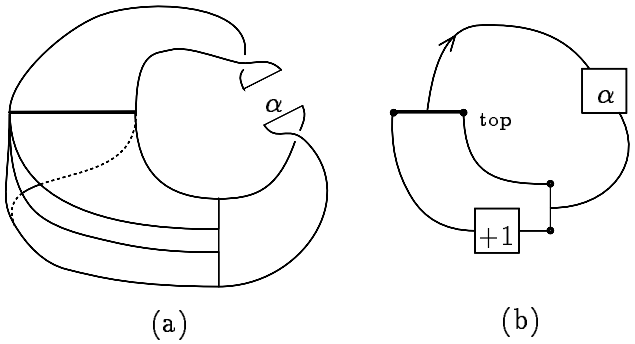

FIGURE 21: (a) the generalized horseshoe template $\mathcal{H}_\alpha$ near , ; (b) the spine $sp(\mathcal{H}_\alpha)$

We stress that for a given system, the global twisting M and the minimum depth i of a horseshoe are uncomputable; hence, one cannot conclude the rigorous existence of any *particular* $\mathcal{H}_\alpha$ for a fixed system, but only for α greater than some unknown lower bound. For example, one cannot assume that the standard horseshoe template $\mathcal{H} = \mathcal{H}_0$ of §2 lives near , , since the minimal local and global twisting may be nonzero. From this, one might conclude that the prior study of knots on $\mathcal{H}$ [HW85, Hol86, Hol89] is unfruitful; however, a study of nonisotopic renormalizations of $\mathcal{H}$ reveals [GHS95] that for n suf-

ficiently large, an isotopic copy of $\mathcal{H}_n$ exists as a subtemplate of $\mathcal{H}$ (see also Prop. 15 of [GH93]). In some sense, then, the simple template $\mathcal{H}$ contains much (but not all!) of the topological complexity of the full Shil'nikov spiral.

Additional issues concerning how knots on these various horseshoes are linked about one another, and even what a good definition of linking for templates is, remain open questions. The analysis of this appendix is an initial survey of this complicated structure in phase space.

The horseshoe templates $\mathcal{H}_\alpha$ which occur near , are not terribly complicated, and can be easily visualized as in Fig. 21. However, not all templates which we will encounter in this appendix are so docile. We thus introduce a shorthand notation for picturing a template, using the horseshoe templates as examples.

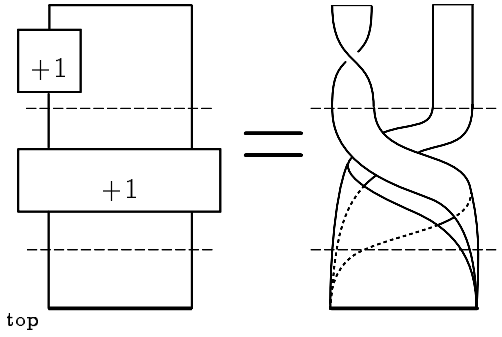

FIGURE 22: Integers in the boxes denote twisting

Instead of representing a template $\mathcal{T}$ as a collection of two-dimensional strips which join together at branch lines, we will collapse each strip in the direction transverse to the semiflow, leaving the branch lines intact. This will reduce $\mathcal{T}$ to a one-dimensional *spine*, $sp(\mathcal{T})$, which captures most of the topological features of $\mathcal{T}$. To encode the twisting of various strips as well as to simplify our notation, we will use "input-output" boxes labeled with integers to denote twisting in individual or in collections of strips: see Fig. 22. We must also keep track of the order in which joining strips overlap at a branch line. We do so by pre-arranging the representation of $\mathcal{T}$ so that strips entering a branch line from left to right (or vice versa) overlap monotonically from top to bottom: this will be represented by a ("top") labeling of the incoming edges at a branch line (see Fig. 21 or 22). *Example:* the template $\mathcal{Z}$ of Proposition 2 and Fig. 15 appears in shorthand form in Fig. 23.

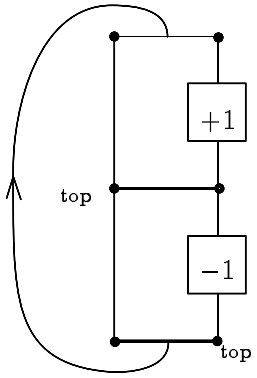

FIGURE 23: The spine for the template $\mathcal{Z}$

With this shorthand notation, the various horseshoes built from the B_i and B_{i+1} boxes are displayed in Fig. 21(b).

We now carry this geometric construction one step further. A careful analysis of the map $\tau_1\tau_0$, details of which can be found in [Wig88, Wig90], verify the following theorem:

Theorem 7 *Under the hypotheses of Theorem 5, there exists, for every integer $N > 1$ an invariant set of the flow in a tubular neighborhood of , which is conjugate to a full shift on N symbols.*

The proof is a (tedious) check of the so-called Conley-Moser conditions [Wig90] on the boxes $\{B_k, B_{k+1}, \ldots, B_{k+N-1}\}$ for k sufficiently large. Geometrically, each B_i will flow near p according to Eqn. (17) and twist about , with each succes-

sive box B_{i+1} incurring an additional half-twist as compared to that of B_i.

The template which results from considering the collection of boxes $\{B_k, B_{k+1}, \ldots, B_{k+N-1}\}$ is quite complicated, and we will of necessity use our shorthand notation. To simplify matters, consider again the derivation of the standard horseshoe template from Fig. 5. In the case of a spiral homoclinic connection, the suspension of the horseshoe map also appears, though with a certain amount of additional twisting. In like manner, the full N-shift appears as a suspended "spiral N-shoe" (cf. [MT93]): a generalization of the Smale horseshoe appearing in Fig. 24.

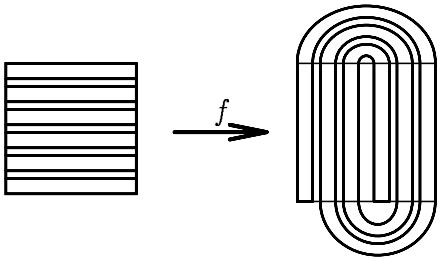

FIGURE 24: The spiral N-shoe ($N = 6$)

We will suspend this map directly and collapse a stable foliation out to obtain a template, which we will then embed in a neighborhood of the fixed point. The stable and unstable foliations of this map are again horizontal and vertical lines, and the suspension can be easily visualized, as was done in Fig. 5. Fig. 25 gives the spine of the resulting template. It is an exercise for the reader to confirm that this spine follows from the suspension. *Hint:* the action of the spiral N-shoe is to perform $N - 1$ half-twists.

This local template model of the flow near a spiral fixed point may then be connected with a strip following , , inserting an unknown (M) number of half-twists to account for the global twisting along , . In addition, we cannot assume that the box B_0 is hyperbolic, as in Fig. 20: we must "prune" away the first k strips for some k

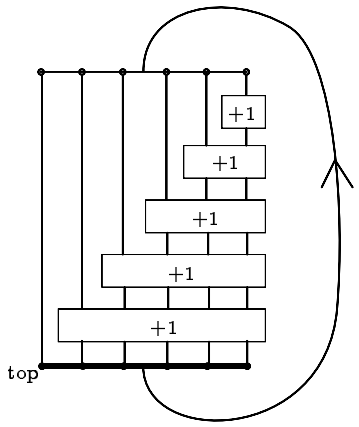

FIGURE 25: The spiral N-shoe template ($N = 6$)

which depends upon the particular flow. Having done this, we give the spine-form of the full N-shift template which occurs near a single unknotted Shil'nikov homoclinic orbit in Fig. 26 (here $N = 6$).

Since certain features of the template in Fig. 26 are a priori uncomputable, general statements concerning the knot and link structure of orbits near , are difficult to make. One might hope for results similar to the case of the $\mathcal{H}_\alpha$, in which more complicated versions are contained as subtemplates of simpler templates: this however is beyond the scope of the present analysis. We should further emphasize that the template of Fig. 26 does not capture *all* the orbits near a spiral homoclinic connection, but merely those which live in a convenient hyperbolic subset of the flow.

A.2 Symmetric spiral connections

When passing to a symmetric configuration as in Fig. 13, many of the problems involving additional twisting that one encounters in constructing templates for single connections disappear. This will allow us to conclude the existence of

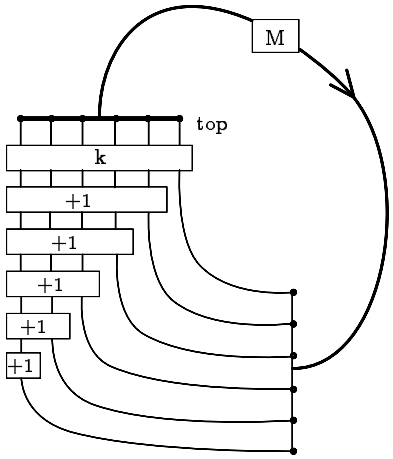

FIGURE 26: The full N-shift template ($N = 6$) near ,

the template $\mathcal{Z}$, completing the proof of Proposition 2.

Recall the order-two symmetries we consider, given in Eqn. (13). We will begin with a treatment of the symmetry $\Psi : (x, y, z) \mapsto (-x, -y, z)$. In this case, we have an unknotted heteroclinic cycle joining p to $\tilde{p} \equiv \Psi(p)$. We have four different "zones" which describe the flow near the heteroclinic cycle: the flows in a neighborhood of p and $\tilde{p}$, and in a tubular neighborhood of , and $\tilde{\ }$, $\equiv \Psi(\ ,\ )$.

The analysis of a pair of Shil'nikov connections under the symmetry Ψ proceeds as in the single-spiral case: erect the Poincaré sections Π_0 and Π_1 as well as their images ($\tilde{\Pi}_0$ and $\tilde{\Pi}_1$) under Ψ. There are return maps,

$$\begin{aligned} \tau_0 &: \Pi_0^+ \to \Pi_1 \\ \tau_1 &: \Pi_1 \to \tilde{\Pi}_0 \\ \tilde{\tau}_0 = \Psi\tau_0\Psi &: \tilde{\Pi}_0^+ \to \tilde{\Pi}_1 \\ \tilde{\tau}_1 = \Psi\tau_1\Psi &: \tilde{\Pi}_1 \to \Pi_0. \end{aligned} \tag{23}$$

The analysis of the ensuing return maps is identical, except that the full return map on Π_0^+ is given as $\tilde{\tau}_1\tilde{\tau}_0\tau_1\tau_0$.

Since the flow local to p and $\tilde{p}$ is identical to the single-spiral case, we may construct local N-shift templates as per the previous section by looking at the boxes $\{B_i\}$ and their counterparts $\{\tilde{B}_i\}$ under Ψ. In this case, since there are two fixed points near which the boxes are stretched and folded, there will be two branch lines in the induced templates. Again, the global connecting maps τ_1 and $\tilde{\tau}_1$ are affine, so we may represent their contribution to the template as strips which connect the template structures local to p and $\tilde{p}$. As before, there will be some mandatory local twisting of the boxes B_i (and their images under Ψ) which manifests itself as a minimal i for which B_i forms a proper horseshoe. And in addition, there will be a fixed number, M, of half-twists along , from Π_1 to $\tilde{\Pi}_0$.

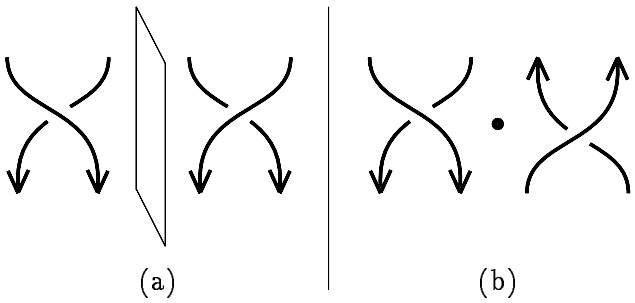

FIGURE 27: (a) crossings under the symmetry $(x, y, z) \mapsto (-x, -y, -z)$ (b) crossings under the symmetry $(x, y, z) \mapsto (-x, -y, -z)$

A key observation is this: because of the symmetry Ψ, the crossing type (positive or negative) is *reversed* under application of Ψ (see Fig. 27 and cf. Fig. 9). That is, if the M half-twists along , are of positive sign, then the (precisely) M half-twists along $\tilde{\ }$ are of negative sign. Similarly, the local templates constructed near p reverse all crossings at $\tilde{p}$. Hence, the coupled N-shift template appears as in Fig. 28 (spine form). We note again that one cannot *a priori* say what the minimal k is such that the boxes B_k satisfy the hyperbolicity requirements, or what M is.

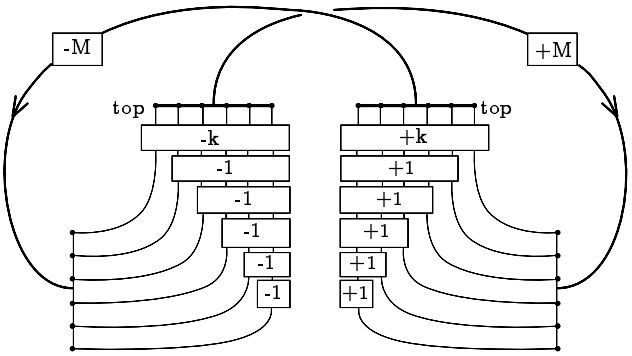

FIGURE 28: The coupled N-shift template along , and $\Psi(,)$

We will manipulate this spine (and others) under the following rules:

1. Even numbers of half-twists of opposite signs cancel, without affecting any crossings in between them.
2. A pair of odd half-twists of opposite signs "flips" what lies between them.
3. An even number of half-twists commute with all other braiding and twisting.

The interested reader may verify these statements with a belt, or by studying the commutator subgroup of the braid groups [Bir74].

Proposition 4 *The template $\mathcal{Z}$ appears as a subtemplate of the coupled N-shift template ($N \geq 2$) for the Ψ-symmetric heteroclinic loop.*

Proof: Given the template of Fig. 28, we will construct our subtemplate by ignoring all but four strips of the template. Consider again the boxes B_i and $\tilde{B}_i$ which collapse into the strips of the template. Assume without loss of generality that the global configuration of , and ˜ appears as in Fig. 28: that is, there is a crossing of , over ˜ which is of positive sign. Then, for i sufficiently large to ensure hyperbolicity, choose the boxes B_i, B_{i+1}, $\tilde{B}_{i+2}$, and $\tilde{B}_{i+3}$, where the parity of i is *opposite* the parity of M. These boxes are then collapsed into template strips and connected to form a template with spine given in Fig. 29(a). First, we "straighten-out" the template, replacing the crossing with two half-twists, as per Fig. 29(b). This offsets the difference in $+i$ and $-i-2$. Next, the twisting due to M and $-i$ ($-M$ and i resp.) is consolidated in Fig. 29(c). Since M and i are of opposite parity, $M - i = 2n + 1$ for some n. Likewise, $i - M = -2n - 1$, and the even numbers of twists cancel completely. The remaining $+1$ and -1 twists cancel, "flipping" a portion of the spine, yielding Fig. 29(d). This is the precisely the spine for $\mathcal{Z}$ as displayed in Fig. 23. □

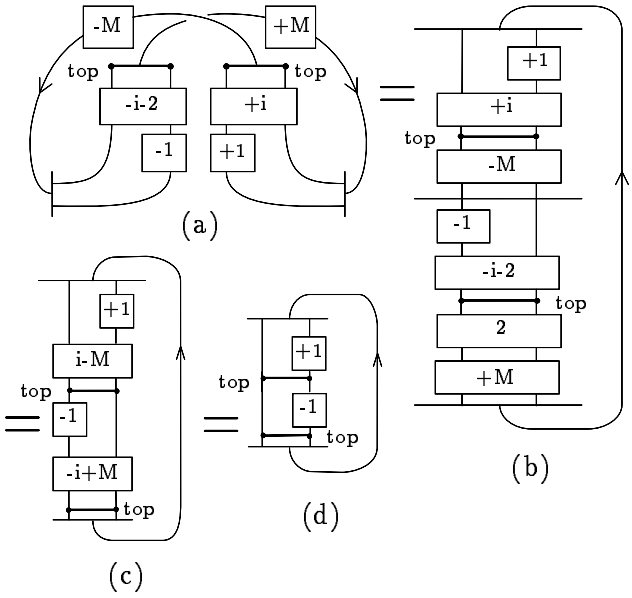

FIGURE 29: A reduction to the template $\mathcal{Z}$

Remark: of course, there are a countable infinity of disjoint copies of $\mathcal{Z}$ living within this configuration, obtained by choosing i arbitrarily high. The use of symmetry to cancel twisting is of great assistance here.

Next, we consider the symmetry $\Psi : (x, y, z) \mapsto (-x, -y, -z)$ associated with either the double-

homoclinic or the heteroclinic configurations (see Fig. 13). The analysis for this case is quite similar to that of the previous symmetric case — the Poincaré sections Π_0 and Π_1, along with their images under Ψ, are erected and local and global return maps are derived. The interested reader may find more complete constructions in [Wig88, Tre84]. Note that, in the double homoclinic case, we are "ignoring" the additional interactions between the maps and considering only that portion of the flow which alternates between following the connections , and $\tilde{,} = \Psi(,)$. We will treat this issue shortly.

As before, we use the model for a local N-shift template at a spiral fixed point (see Fig. 26) and connect the ends along the global connections in order to obtain a full template for the flow. The only difference between this configuration and the one of the previous case is the placement of the local spiral template — whether or not to "flip it over". Fig. 30 gives the coupled N-shift template for the spiral configurations under Ψ. Again, we call the reader's attention to the fact that there exist $\pm M$ half-twists along , and $\tilde{,}$, and that there is some mandatory local twisting, given by the smallest i such that B_i is hyperbolic.

Proposition 5 *The template $\mathcal{Z}$ appears as a subtemplate of the coupled N-shift template ($N \geq 2$) for the Ψ-symmetric double-homoclinic or heteroclinic loop.*

Proof: As in Proposition 4, we ignore all but four boxes. In this case, choose B_i, B_{i+1}, and their images under Ψ: $\tilde{B}_i$ and $\tilde{B}_{i+1}$. Choose i so that it is sufficiently large and has the same parity as M. Then Fig. 31(a) gives the subtemplate formed by these strips, which is "straightened-out" in Fig. 31(b). Note that, since i and M are of the same parity, they coalesce to form an even number of twists, as displayed in Fig. 31(b). Since even numbers of twists cancel, we are left with Fig. 31(d), which is the spine for $\mathcal{Z}$. □

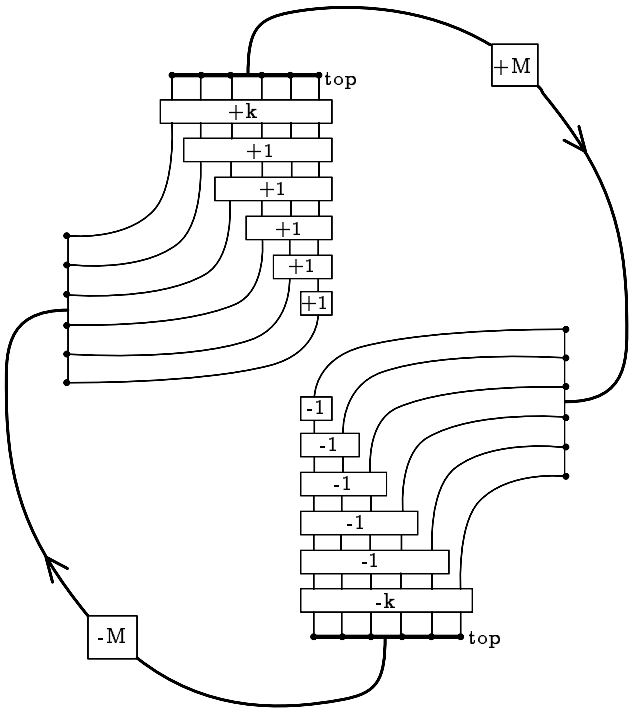

FIGURE 30: The coupled N-shift template along , and $\Psi(,)$

This concludes the proof of Proposition 2, which is used to show the existence of (apparently) simple structures in phase space which force all knots and links.

We conclude with one last template classification. In the symmetric configuration in which there is a double homoclinic connection at $p = \Psi(p)$, the return maps are "entwined": that is, τ_0 acts on *all* of Π_0, and not just Π_0^+ (the same holds for $\tilde{\tau}_0$ and $\tilde{\Pi}_0$). The maps τ_0 and $\tilde{\tau}_0$ are discontinuous maps which act as follows:

$$\begin{aligned} \tau_0 &: \begin{matrix} \Pi_0^+ \to \Pi_1 \\ \Pi_0^- \to \tilde{\Pi}_1 \end{matrix} \\ \tilde{\tau}_0 &: \begin{matrix} \tilde{\Pi}_0^+ \to \tilde{\Pi}_1 \\ \tilde{\Pi}_0^- \to \Pi_1 \end{matrix} \\ \tau_1 &: \Pi_1 \to \Pi_0 \\ \tilde{\tau}_1 &: \tilde{\Pi}_1 \to \tilde{\Pi}_0. \end{aligned} \tag{24}$$

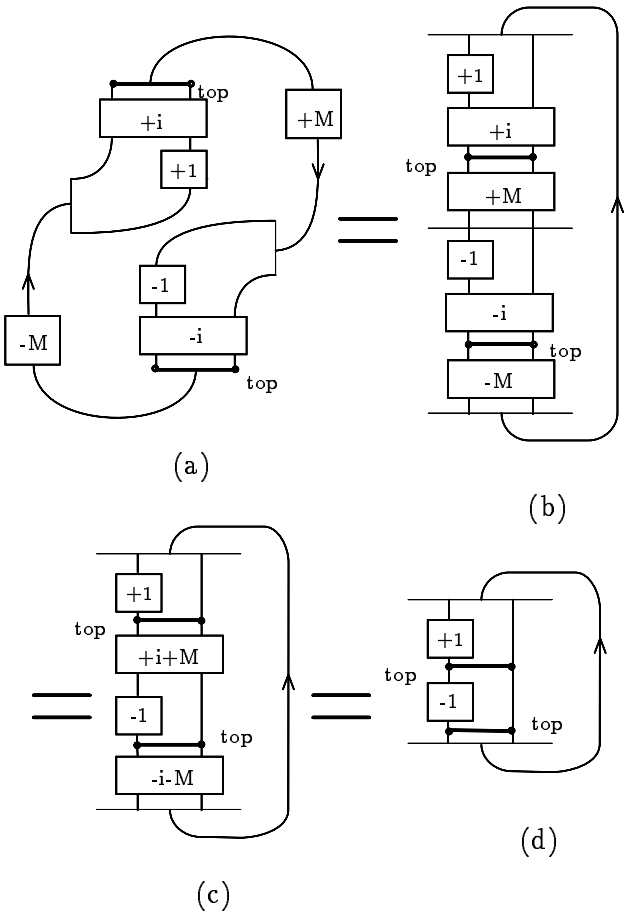

FIGURE 31: A reduction to the template $\mathcal{Z}$

The linear approximation to the flow near p is the same as in the single spiral case previously examined; however, the geometry of the mixing of the flow near , and , in a neighborhood of p is extremely complicated. We leave the reader with the spine of one last template, formed from looking at boxes $\{B_i\}$ in each of the four half-planes $\Pi_0+, \Pi_0^-, \tilde{\Pi}_0^+$, and $\tilde{\Pi}_0^-$. Fig. 32 exhibits the complicated structure.

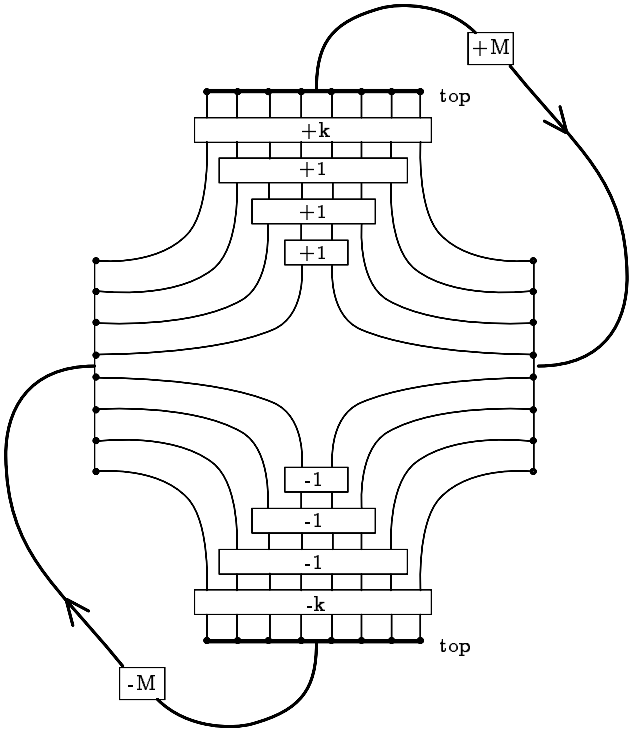

FIGURE 32: The full template for a double-spiral homoclinic configuration

REFERENCES

[ACT81] A. Arnéodo, P. Coullet, and C. Tresser. Possible new strange attractors with spiral structure. *Commun. Math. Phys.*, 79:573–579, 1981.

[Ale23] J. W. Alexander. A lemma on systems of knotted curves. *Proc. Nat. Acad. Sci. USA*, 9:93–95, 1923.

[BC92] V. Belykh and L. Chua. New type of strange attractor from a geometric model of Chua's circuit. *Int. J. Bif. Chaos*, 2(3):697–704, 1992.

[Bir74] J. Birman. *Braids, Links, and Mapping Class Groups.* Princeton University Press, Princeton, N.J., 1974.

[Bow78] R. Bowen. On Axiom A diffeomorphisms. In *Regional Conference Series in Mathematics 35*, pages 1–45. National Science

Foundation, American Mathematical Society, 1978.

[Boy84] P. Boyland. Braid types and a topological method for proving positive entropy. Preprint, 1984.

[Boy94] P. Boyland. Topological methods in surface dynamics. *Topology and its Applications*, 58:223–298, 1994.

[BW83a] J. Birman and R. F. Williams. Knotted periodic orbits in dynamical systems–I : Lorenz's equations. *Topology*, 22(1):47–82, 1983.

[BW83b] J. Birman and R. F. Williams. Knotted periodic orbits in dynamical systems–II : knot holders for fibered knots. *Cont. Math.*, 20:1–60, 1983.

[BZ85] G. Burde and H. Zieschang. *Knots*. De Gruyter, Berlin, 1985.

[CDF90] S. N. Chow, B. Deng, and B. Feidler. Homoclinic bifurcation at resonant eigenvalues. *J. Dyn. Diff. Eqs.*, 2(2):177–244, 1990.

[Cha93] A. Champneys. Homoclinic tangencies in the dynamics of articulated pipes conveying fluid. *Physica D*, 62:347–359, 1993.

[CKM86] L. Chua, M. Komuro, and T. Matsumoto. The double scroll family. *IEEE Trans. on Circuits and Systems*, 33:1073–1118, 1986.

[Fei78] M. J. Feigenbaum. Quantitative universality for a class of nonlinear transformations. *J. Stat. Phys.*, 19:25–52, 1978.

[FW85] J. Franks and R. F. Williams. Entropy and knots. *Trans. Am. Math. Soc.*, 291(1):241–253, 1985.

[GH83] J. Guckenheimer and P. J. Holmes. *Nonlinear Oscillations, Dynamical Systems, and Bifurcations of Vector Fields*. Springer-Verlag, New York, 1983.

[GH93] R. Ghrist and P. Holmes. Knots and orbit genealogies in three dimensional flows. In *Bifurcations and Periodic Orbits of Vector Fields*, pages 185–239. NATO ASI series C volume 408, Kluwer Academic Press, 1993.

[Ghr95] R. Ghrist. Branched two-manifolds supporting all links. To appear in *Topology*, 1995.

[GHS95] R. Ghrist, P. Holmes, and M. Sullivan. Knots and links in three-dimensional flows. In preparation, December 1995.

[GKN84] P. Gaspard, R. Kapral, and G. Nicolis. Bifurcation phenomena near homoclinic systems: a two-parameter family. *J. Stat. Phys.*, 35:697–727, 1984.

[GS84] P. Glendinning and C. Sparrow. Local and global behavior near homoclinic orbits. *J. Stat. Phys.*, 35:645–698, 1984.

[GS86] P. Glendinning and C. Sparrow. T-points: a codimension two heteroclinic bifurcation. *J. Stat. Phys.*, 43:479–488, 1986.

[GW79] J. Guckenheimer and R. F. Williams. Structural stability of Lorenz attractors. *Inst. Hautes Études Sci. Publ. Math.*, 50:59–72, 1979.

[GW93] J. Guckenheimer and P. Worfolk. Dynamical systems: some computational problems. In *Bifurcations and Periodic Orbits of Vector Fields*, pages 240–277. NATO ASI series C volume 408, Kluwer Academic Press, 1993.

[Hol80] P. J. Holmes. A strange family of three-dimensional vector fields near a degenerate singularity. *J. Diff. Eq.*, 37(3):382–403, 1980.

[Hol86] P. J. Holmes. Knotted periodic orbits in suspensions of Smale's horseshoe: period mutiplying and cabled knots. *Physica D*, 21:7–41, 1986.

[Hol89] P. J. Holmes. Knotted periodic orbits in suspensions of Smale's horseshoe: extended families and bifurcation sequences. *Physica D*, 40:42–64, 1989.

[HW85] P. J. Holmes and R. F. Williams. Knotted periodic orbits in suspensions of Smale's horseshoe: torus knots and bifurcation sequences. *Archive for Rational Mech. and Anal.*, 90(2):115 –193, 1985.

[KDTC94] Lj. Kocarev, D. Dimovski, Z. Tasev, and L. Chua. Topological description of a chaotic attractor with spiral structure. *Phys. Lett. A*, 190:399–402, 1994.

[KRC93] A. Khibnik, D. Roose, and L. Chua. On periodic orbits and homoclinic bifurcations in Chua's circuit with a smooth nonlinearity. *Int. J. Bif. and Chaos*, 3(2):363–384, 1993.

[Lor63] E. N. Lorenz. Deterministic non-periodic flow. *J. Atmospheric Sci.*, 20:130–141, 1963.

[Los94] J. Los. Knots, braid index, and dynamical type. *Topology*, 33(2):257–270, 1994.

[MM95] K. Mischaikow and M. Mrozek. Chaos in the Lorenz equations: a computer-assisted proof. *Bull. Am. Math. Soc.*, 32(1):66–72, 1995.

[Mor78] J. Morgan. Nonsingular Morse-Smale flows on 3-dimensional manifolds. *Topology*, 18:41–54, 1978.

[MSN+91] G. B. Mindlin, H. S. Solari, M. A. Natiello, R. Gilmore, and X. J. Hou. Topological analysis of chaotic time series data from the Belousov-Zhabotinskii reaction. *J. Nonlinear Sci.*, 1:147–173, 1991.

[MT77] J. Milnor and W. Thurston. On iterated maps of the interval I and II. Unpublished notes, Princeton University, 1977.

[MT93] F. A. McRobie and J. M. T. Thomson. Braids and knots in driven oscillators. *Int. J. Bifurcation and Chaos*, 3:1343–1361, 1993.

[PTT87] I. Procaccia, S. Thomae, and C. Tresser. First-return maps as a unified renormalization scheme for dynamical systems. *Phys. Rev. A*, 35 (4):1884–1900, 1987.

[Rol77] D. Rolfsen. *Knots and Links.* Publish or Perish, Berkely, CA, 1977.

[Shi65] L. P. Shil'nikov. A case of the existence of a countable number of periodic motions. *Soviet Math. Dokl.*, 6:163–166, 1965.

[Shi70] L. P. Shil'nikov. A contribution to the problem of the structure of an extended neighborhood of a rough equilibrium state of saddle-focus type. *Math. USSR Sbornik*, 10(1):91–102, 1970.

[Sma67] S. Smale. Differentiable dynamical systems. *Bull. Am. Math. Soc.*, 73:747–817, 1967.

[Sul94] M. C. Sullivan. The prime decomposition of knotted periodic orbits in dynamical systems. *J. Knot Thy. and Ram.*, 3(1):83–120, 1994.

[Tre84] C. Tresser. About some theorems by L. P. Shil'nikov. *Ann. Inst. H. Poincaré*, 40:441–461, 1984.

[Tuf94] N. B. Tufillaro. Topological organization of (low dimensional) chaos. In J. P. Nadal and P. Grassberger, editors, *From Statistical Physics to Statistical Inference and Back.* NATO ASI series C, Kluwer Academic Press, 1994.

[Wad89] M. Wada. Closed orbits of nonsingular Morse-Smale flows on S^3. *J. Math. Soc. Japan*, 41(3):405–413, 1989.

[Wic93] F. J. Wicklin. *Dynamics near resonance in multi-frequency systems.* PhD thesis, Cornell University, 1993.

[Wig88] S. Wiggins. *Global Bifurcations and Chaos: Analytical Methods.* Springer-Verlag, Berlin, Heidelberg, New York, 1988.

[Wig90] S. Wiggins. *Introduction to Applied Nonlinear Dynamical Systems and Chaos.* Springer-Verlag, Berlin, Heidelberg, New York, 1990.

[Wil74] R. F. Williams. Expanding attractors. *Inst. Hautes Études Sci. Publ. Math.*, 43:169–203, 1974.

[Wil77] R. F. Williams. The structure of Lorenz attractors. In S. Smale A. Chorin, J. E. Marsden, editor, *Turbulence Seminar, Berkeley 1976/77*, pages 94–116. Springer Lecture Notes in Math. Vol. 615, 1977.

[Wil79] R. F. Williams. The structure of Lorenz attractors. *Inst. Hautes Études Sci. Publ. Math.*, 50:73–79, 1979.